文章编号:1000-0887(2016)12-1308-16

Application of Sound Source Models to the Heated Subsonic Jet*

ZHANG Xing-chen, YANG Hai-hua, WAN Zhen-hua, SUN De-jun

(*Department of Modern Mechanics, University of Science and Technology of China, Hefei* 230027, *P.R.China*)

Abstract: The noise generation mechanisms associated with instability waves in the heated subsonic transitional jet are studied, which are compared with its cold counterpart. The spatial evolution of instability waves is obtained by solving linear parabolized stability equations (LPSE) based on the time-averaged flow field of the large eddy simulation (LES). Then, the linear and nonlinear models for jet noise are built based on the LPSE solutions, coupled with the acoustic analogy. The LPSE results show that heating increases the spatial growth rate and leads to earlier saturation. For high-frequency components, the sound pressure levels (SPL) are raised by heating as shown in the linear model. In general, compared with that for the cold jet, the gap of SPL between the linear model and the LES is reduced for the heated jet, which indicates that the linear mechanism plays a more important role in the hot jet. For a cold subsonic jet, previous studies have shown that the nonlinear model is able to raise acoustic efficiency. Here, it is found that the gap of SPL between the nonlinear model and the LES could be further decreased in the hot jet, and the thermodynamic sound source terms play a bigger role.

Key words: LPSE; instability wave; linear mechanism; nonlinear mechanism

CLC number: O35 **Document code**: A

doi: 10.21656/1000-0887.370526

Introduction

The noise generated by turbulent jets has been regarded as a significant problem in aeroacoustics over decades. However, based on the acoustic analogy theory, the understanding of sound sources defined in acoustic analogy equations is limited[1]. Usually, jet noise is believed to be produced by 2 components, one is the large-scale coherent structure and the other is the fine-scale turbulence, based on the experiment results of Tam et al. (2008)[2]. They considered fine-scale turbulence associated with the sound field in sideline directions. And the large-scale coherent structures, which were first proposed by Bishop et al. (1971)[3] and Tam (1971)[4], are believed to be the major source for the sound radia-

* Received 2016-11-03; Revised 2016-11-26

Project supported by the National Natural Science Foundation of China (11232011; 11402262; 11621202)

First author, ZHANG Xing-chen, E-mail: zxczxc@mail.ustc.edu.cn

Corresponding author, WAN Zhen-hua, E-mail: wanzh@ustc.edu.cn

tion at small polar angles. It is generally recognized that the hydrodynamic properties of large-scale structures, such as convection speeds, are closely related to the evolution of instability waves, as shown in the experiment evidence of Suzuki & Colonius (2006)[5]. Recently, a great deal of efforts have been made to investigate the near-field "wave-packet" and far-field sound (Jordan & Colonius (2013), Cavalieri et al. (2011, 2013, 2014), Rodríguez et al. (2015))[6-11]. However till now, to predict far-field sound based on simple models or reasonable wave-packets in subsonic turbulent jets is still a tough task.

According to the linear stability theory (LST), in subsonic jets, the phase speed is usually subsonic and the instability modes cannot radiate far-field sound directly. The parallel flow assumption of the LST neglects any streamwise changes in the mean flow (Cheung (2007))[12]. In view of the non-parallel effect, the parabolized stability equations (PSE) have been developed since the late 1980's (Bertolotti et al. (1991, 1992))[13-14]. Recently, the far-field sound can be well-predicted with the PSE in supersonic jets (Rodríguez et al. (2012), Sinha et al. (2014))[15-16]. However, in subsonic jets, results calculated with the PSE method still can't agree with the experimental or DNS results. Some missing aspects, such as the nonlinear mechanism[17-18], intermittency and coherency decay etc., might play important roles in sound radiation.

In this work, we focus on examining the linear and nonlinear flow responses and noise generation in the heated jet with the same Mach number, compared to the cold jet in our previous work[1]. The large-eddy simulation is carried out to obtain the flow field, and based on the LES database, the far-field sound is calculated with Kirchhoff's method. Considering the non-parallel effect, the parabolized stability equations are solved for characterizing instability wave evolution. The linear and nonlinear interaction models tested in ref. [1] are also constructed based on the PSE solutions. This paper extends both sound source models to the heated jet, and also analyzes sound generation mechanisms associated with heating.

The rest of this paper is organized as follows. In section 1, the primary numerical approaches and jet parameters used in this work are introduced briefly. Subsection 2.1 gives a detailed description of the LES database of 2 jets including flow field and far-field sound. In subsection 2.2, we compare the role of instability waves between the cold and heated jets, from both PSE and LES results. In subsections 2.3 and 2.4, the linear and nonlinear models are extended to the heated jet, and quantitative comparison of far-field sound pressure levels between the simplified models and LES data is also carried out. Importantly, the effect of heating is considered across whole section 2, and some discussions are also made. In section 3, the major conclusions are summarized.

1 Numerical method and flow parameters

1.1 Large eddy simulation database

An LES database of 2 subsonic turbulent round jets with different temperature ratios is used in the present work. The flow parameters are listed in table 1. The case M08T086 re-

fers to the cold jet, and the case M08T176 represents the heated one. Note that these 2 jets have the same Mach number 0.83 and the same Reynolds number 10^5. In the inflow buffer-zone of both jets, multiple eigenmodes with different frequencies and azimuthal wavenumbers are summed as the inflow forcing. More details of the numerical methods can be found in our previous work(Wan et al.(2016, 2013))[1, 19].

Table 1 Parameters of the cold and heated jets in computation

case	U_j/a_∞	T_j/T_∞	U_j/a_j	$Re = \rho_j U_j D/\mu_j$
M08T086	0.83	0.86	0.895	10^5
M08T176	0.83	1.76	0.626	10^5

1.2 Linear parabolized stability equations

The linear parabolized stability equations are applied in modeling instability waves of turbulent jets. The nonparallel effect and the streamwise evolution of instability waves, which would not be included in the linear stability theory, can both be considered in the PSE. In the cylindrical coordinates (r, θ, z), the flow field of jets is described as $\boldsymbol{q} = (\rho, u_z, u_r, u_\theta, T)^{\mathrm{T}}$, which represent the density, the axial, radial and azimuthal velocities and the temperature. The flow variables can be decomposed to mean and disturbance components, and the disturbance component can be written as the product of the amplitude function and the exponential function as follows:

$$\boldsymbol{q}' = \hat{\boldsymbol{q}}(z,r)\exp\left[\mathrm{i}\left(\int_{z_0}^{z}\alpha(\xi)\,\mathrm{d}\xi + m\theta - \omega t\right)\right], \tag{1}$$

where, α is the complex streamwise wavenumber, m is the azimuthal wavenumber, and ω is the angular frequency. Introduce eq.(1) into the compressible Navier-Stokes equations, with the PSE assumption, one can obtain the following disturbance equation:

$$\left[\boldsymbol{M}\frac{\mathrm{d}}{\mathrm{d}z} - \omega\boldsymbol{K} + \boldsymbol{L}\right]\hat{\boldsymbol{q}}(z,r) = \frac{F_{\mathrm{N}}}{A}, \tag{2}$$

where, matrices $\boldsymbol{M}$, $\boldsymbol{L}$, $\boldsymbol{K}$ which are associated with mean flow variable $\bar{\boldsymbol{q}}$ are all linear operators. The detailed formulation of these operators can be seen in Cheung(2007)[12]. In the linear parabolized stability equations, nonlinear item F_{N} on the right-hand side is set to 0.

In order to solve eq.(2), an additional constraint must be introduced, with the initial condition from the eigenmodes of LST equations. Following Cheung(2007)[12], a normalized condition is proposed to limit the rapid change in the eigenfunctions:

$$\int_0^{R_{\max}} \hat{v}_z^* \frac{\partial \hat{v}_z}{\partial z} r\,\mathrm{d}r = 0. \tag{3}$$

A downstream marching algorithm is developed to solve the LPSE, with the initial condition of eigenvalues and eigenfunctions from linear stability results at $z = 0$. The LST results show that the heated jet has higher growth rate and lower corresponding frequencies. Previous studies, such as Herbert(1997)[20], have shown that the minimum mesh step size in the streamwise direction is limited to a certain value, below which it would cause strong numerical instabilities. Following Andersson et al.(1998)[21], a modified formulation of the LPSE is applied:

$$\left[\boldsymbol{M}'\frac{\mathrm{d}}{\mathrm{d}z}-\omega\boldsymbol{K}+\boldsymbol{L}\right]\hat{\boldsymbol{q}}(z,r)=\frac{F_{\mathrm{N}}}{A}, \tag{4}$$

where, $\boldsymbol{M}'=\boldsymbol{M}+s(-\omega\boldsymbol{K}+\boldsymbol{L})$, and s is the parameter to control the minimum mesh step size in the streamwise direction.

1.3 Lilley-Goldstein's acoustic analogy

According to Lilley (1974)[22] and Goldstein (2001)[23], the Navier-Stokes (Euler) equations are rearranged, and a 3rd-order wave equation with a simple source term is obtained, which consists of a velocity quadrupole plus a fluctuating temperature dipole. By introducing the new pressure-based variable $\pi\equiv(p/p_0)^{1/\kappa}-1$, the final form of Lilley-Goldstein's equation could be written as

$$\bar{L}_{\mathrm{o}}\pi=\frac{\mathrm{D}_o}{\mathrm{D}t}\frac{\partial f_i}{\partial x_i}-2\frac{\partial U}{\partial x_j}\frac{\partial f_j}{\partial x_1}, \tag{5}$$

where, the right-hand side acts as the noise source term, $x_i(i=1,2,3)$ represents the 3 directions in the Cartesian coordinate system, where x_1 is the streamwise direction, $\bar{L}_{\mathrm{o}}$ is the Pridemore-Brown operator, $\mathrm{D}_o/\mathrm{D}t$ is the convective derivative based on the mean flow velocity and f_i is the externally applied force with respect to the perturbation of velocity and sound speed. The detailed expressions of these operators can be found in Goldstein (2001)[23] and Wan et al. (2016)[1].

In the present work, a Green's function-based method with the Fourier transform of eq.(5) in time domain is applied to solve the Lilley-Goldstein's equation. The detailed information of this method can be seen in Ray et al. (2007)[24]. The eigenmodes of the LPSE solutions are applied to construct the sound source in the right-hand side of eq.(5).

2 Results and discussions

2.1 Description of LES database

We start with the detailed description of the mean flow field and far-field sound pressure level of the 2 jets calculated through large-eddy simulation. Time-averaged axial velocity fields for both cold and heated jets are shown in fig. 1. The computation results show that the potential core length becomes shorter as the temperature increases. These 2 time-averaged mean flow fields are used to calculate the LPSE solutions. The far-field sounds of both jets for $R=60r_0$ at the jet outlets, where r_0 is the jet radius, are calculated with Kirchhoff's method[25]. Fig. 2(a) gives a comparison of the overall sound pressure levels (OASPL) with respect to polar angle θ to the jet axis with the existent experiment data[26-28], and in fig. 2(b) and (c), the sound spectra for $R=60r_0$ compared with previous experiment data[29-30] are displayed. Our computation results are basically in agreement with the experimental data. The sound spectra show broadband peaks at low frequencies in both jets, and the heated jet has a 5 dB higher SPL and a lower peak frequency than the cold jet. At high frequencies $Sr>1$, where Sr is the Strouhal number ($Sr=\omega D_j/(2\pi U_j)$), the SPL in the heated jet becomes lower than in the cold jet, as is found in Suponitsky et al. (2011)[31].

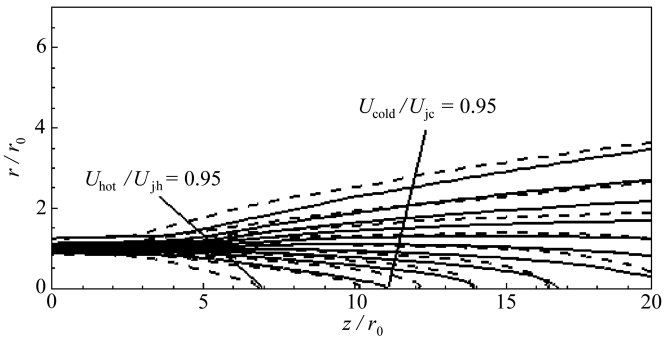

Fig. 1 Axial velocity contours of the mean flow fields in the cold and heated jets

In fig. 2(a), it is found that the OASPL of each jet reaches a peak at a polar angle near $\theta = 30°$, and the heated jet has a bit higher maximum polar angle. In addition, heating increases the noise intensity at polar angles $\theta < 70°$, but reduces the noise intensity at angles $\theta > 70°$. We suppose that the lower noise intensities at high polar angles in the heated jet might be attributed to the reduction of fluctuation intensities in the turbulent mixing region, and the 1~3 dB increase of the OASPL at low polar angles might be associated with different roles of instability waves in the heated jet. As a result, for modelling the evolution of instability waves, the linear parabolized equations are applied to the flow fields of both jets, which would be discussed in the next section.

2.2 Instability waves

In order to clarify the detailed roles of instability waves, the linear parabolized stability equations, based on the time-averaged mean flow field of the LES database, are solved with different m and Sr values. In addition, the discrete Fourier transformation (DFT) is performed for the LES data. Here, the first 2 azimuthal modes, $m = 0$ and $m = 1$, which have the highest energy among all modes, are examined, and the streamwise evolutions of the disturbance kinetic energy (DKE) for specific (Sr, m) from both linear PSE and LES results are shown in fig. 3.

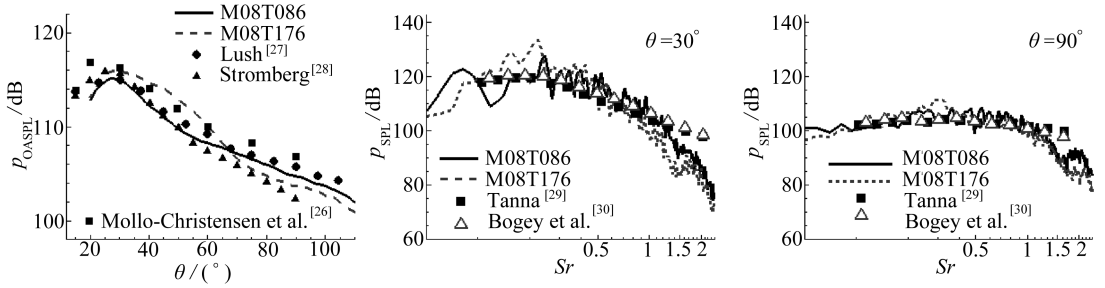

(a) The overall SPL versus polar angle θ (b) The sound pressure spectrum at $\theta = 30°$ (c) The sound pressure spectrum at $\theta = 90°$

Fig. 2 Comparison of far-field sounds for $R = 60r_0$ between the LES and the experiments (the results of cold jet come from ref. [1])

It is found from fig. 3 that the growth of the disturbance kinetic energy of both jets

predicted by the linear PSE is in agreement with the LES results at the linear stage for relative higher frequencies. But there are still some differences at the nonlinear stage. In other words, the linear PSE could not predict the coherent decay downstream at the end of the potential core. In addition, the linear PSE under-predicts the disturbance energy of low-frequency components greatly, e.g. $Sr = 0.2$ in fig. 3(a) and (b), which suggests that nonlinear interactions might cause the existence of this gap.

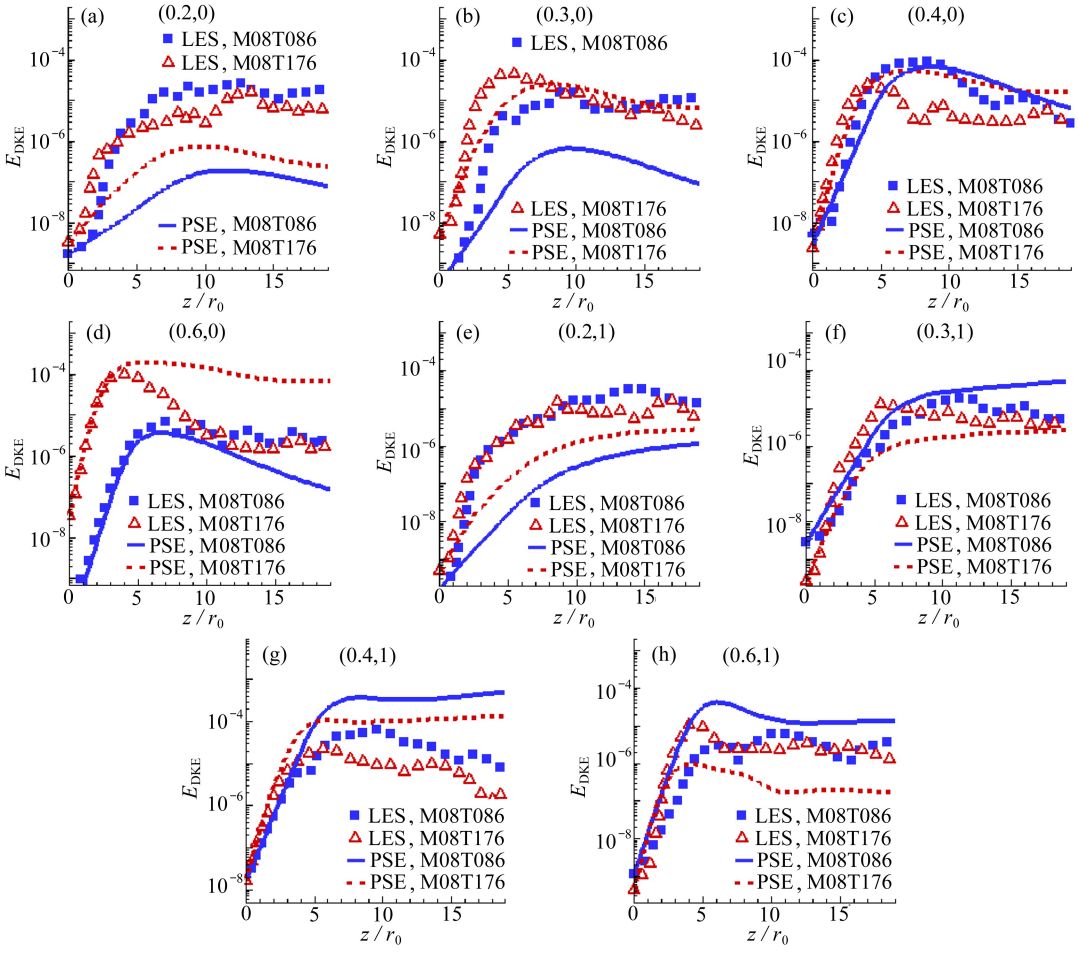

Fig. 3 The discrete kinetic energy(DKE) along the flow direction for different frequencies and azimuthal numbers (Sr, m) in the cold and heated jets

2.3 Linear model for far-field sound

As mentioned above, it is found that the linear PSE could capture the growth of instability waves at the linear stage. In order to investigate the effect of linear mechanism on the sound radiation, we here mainly concentrate on the beam pattern and sound pressure levels of far field sound generated by a single PSE mode in both cold and heated jets. Kirchhoff's method is also applied to the calculation of the far-field sound. Note that the LPSE solution decays exponentially in the radial direction, thus the pressure disturbance at Kirch-

hoff's surface $r = R_{KS}$ varies with the radial coordinate. The SPL decreases by about 2 dB as R_{KS} increases by r_0, and this error is negligible for the gap between the linear model and the LES results. Here, according to Cavalieri et al. (2012)[32] and Wan et al. (2016)[1], $R_{KS} = 6r_0$ is chosen for the LPSE linear model.

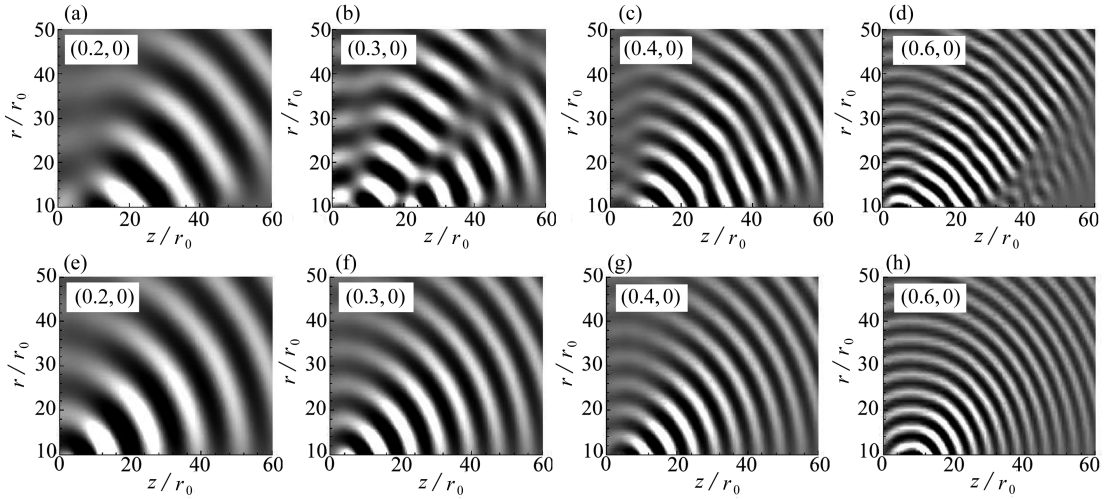

Fig. 4 Contours of sound pressure for different (Sr, m) values in the heated jet ((a)~(d), the LES data; (e)~(h), the linear model results)

Since the linear PSE modes have free amplitudes, here, in order to describe the near-field LPSE wave packets quantitatively, we refer to the previous work of velocity wave packets by Cavalieri et al.(2013)[9]. For axisymmetric mode $m = 0$, the amplitudes of the linear modes are adjusted with LES axial velocity u_z at $z = 4r_0$ on the jet centerline directly. And for $m = 1$, the inner product between LPSE and LES results is defined to determine the free constant for scaling the PSE solutions in both the linear model and the nonlinear model in the next section, to match the LES results. The detailed expression could be seen in Cavalieri et al.(2013)[9].

The contours of acoustic pressure fields of different Sr values for mode $m = 0$ in the linear model comparing to the LES results are shown in fig. 4. The beam patterns of the heated jet show the characteristics of super-directivity, the same as those of the cold jet. It is evident that the dominant sound radiation directions are located at low angles from the jet axis in the linear model. According to the comparison of the beam pattern at the same frequency between the LES and the linear model, the directivity and the maximum radiation angle predicted by the linear model differ greatly from those by the LES. The LES results show multiple acoustic waves radiating downstream, such as the beam pattern in fig. 4(b)~(d), however, in the linear model, only one major direction radiating to low polar angles downstream exists for all frequencies. Compared to the cold jet results in fig. 8 in Wan et al. (2016)[1], the prediction of sound radiation direction becomes even worse in the heated jet. And also, the source locations in the heated jet move upstream, which is con-

sistent with the results in ref. [1]. This indicates that the nonlinear effect in the heated jet might be higher on sound radiation than that in the cold jet, which would be discussed in the next section. Nevertheless, some qualitative laws could be found in the linear model, that the major radiation angles in the hot jet are a bit higher than those in the cold jet for the same Sr, which agrees with the LES results in fig. 2.

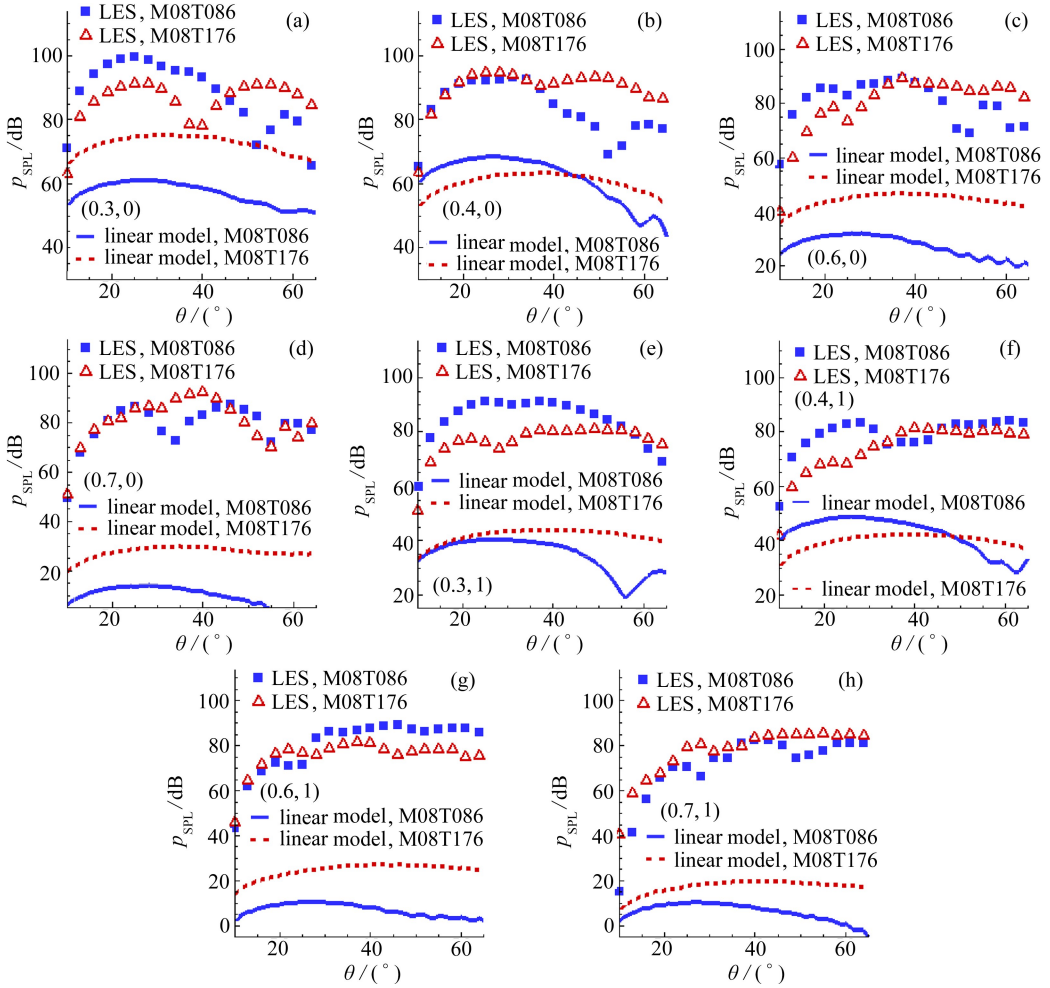

Fig. 5 Comparison of sound pressure level vs. polar angle θ at $R = 60r_0$ for different (Sr, m) values between the linear model and the LES results

Furthermore, the quantitative comparison between the linear PSE model and the LES data is also carried out. The sound pressure levels (SPL) at $R = 60r_0$ for different m and Sr values in both cold and heated jets are shown in fig. 5. Compared to that in the cold jet, the great gap between the LPSE and LES results is reduced to a certain extent for most cases in the heated jet. Note that although the discrepancy appears, the SPL of the heated jet in the linear model is higher than that of the cold jet at high frequencies such as $Sr = 0.6$, 0.7, which is consistent with the higher growth rate of the heated jet predicted by the LST and LPSE, where the linear mechanism plays a more important role in sound generation.

2.4 Nonlinear interaction model for far-field sound

As mentioned above, there is a great gap of far-field sound pressure levels between the linear PSE model and the LES results in present cold and heated jets. Several other mechanisms are involved in sound generation. In Wan et al.(2016)[1], an improved nonlinear model proposed by Sandham et al.(2008)[18] considering weakly nonlinear interaction of instability waves, coupled with Lilley-Goldstein's acoustic analogy, was applied to predict the far-field noise of the cold jet. Here, we extend this model to the heated jet, and concentrate on the effects of heating on the sound sources.

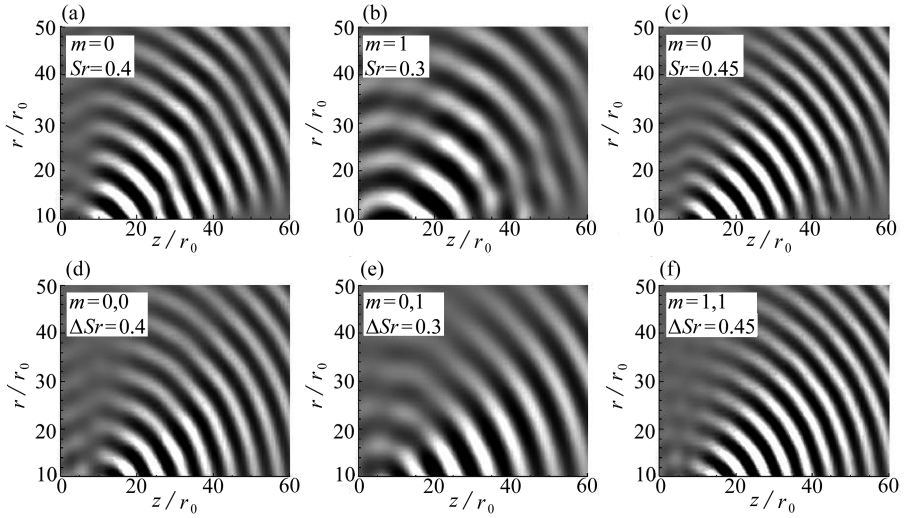

Fig. 6 Contours of sound pressure of the heated jet in the nonlinear model vs. the LES results((a)~(c), the LES data; (d)~(f), the nonlinear model)

In the nonlinear model, the sound source strength can be investigated by means of the amplitude of the mode interactions. We consider the interaction of 2 LPSE modes with azimuthal wavenumbers (m_l, m_n) and real frequencies (ω_j, ω_k). Lilley-Goldstein's equations are introduced here to calculate the far-field sound from instability waves, the source term of which could be constructed with the LPSE modes mentioned above. For instance, the axial quadrupole term can be written as

$$\frac{\partial^2 u_{jl}u_{kn}}{\partial z^2} = \hat{u}_{jl}\hat{u}_{kn}A^{+}_{jkln}\exp(\mathrm{i}[(m_l+m_n)\theta-(\omega_j+\omega_k)t]) + \hat{u}^{*}_{jl}\hat{u}_{kn}A^{-}_{jkln}\exp(\mathrm{i}[(m_l-m_n)\theta-(\omega_j-\omega_k)t]) + c.c., \tag{6}$$

where, $c.c.$ denotes the complex conjugate, A^{+} and A^{-} are the sum and difference mode amplitudes. The expression of A^{-} is given by

$$A^{-}_{jkln} = [\sigma_{jl}+\sigma_{kn}+\mathrm{i}(\alpha_{jl}-\alpha_{kn})]^2\exp\left(\int[\sigma_{jl}+\sigma_{kn}+\mathrm{i}(\alpha_{jl}-\alpha_{kn})]\mathrm{d}z\right), \tag{7}$$

where, α and $-\sigma$ are the real and imaginary parts of the complex wavenumber.

It was found by Sandham et al. (2006)[17] that the difference wavenumber nonlinear interaction mechanism dominated the sound radiation from subsonic instability modes,

which was further clarified in their later work[33]. We consider the difference mode interactions of dominant mode pairs of (0,0), (0,1) and (1,1) in the heated jet. The contours of A^- with respect to Sr of the 2 LPSE modes from 0.1 to 1 are calculated, with the axial positions $z = 10r_0$ in the cold jet and $z = 6r_0$ in the heated jet, both of which are in the vicinity of the end of the potential core.

In the cold jet[1], the peak values of A^- are located at Sr combination (0.75,0.45) in mode pair (0,0), and (0.7,0.4) in mode pairs (0,1) and (1,1), corresponding difference Sr is 0.3 for all modes. However, in the present heated jet, these peaks are shifted to (0.8, 0.4), (0.55, 0.25) and (0.75, 0.3), and the difference mode frequencies are shifted to higher Sr values. We can find that the corresponding peak frequencies increase slightly in the heated jet for mode $\Delta m = 0$, in contradiction to the LES sound spectra results, which will be discussed later.

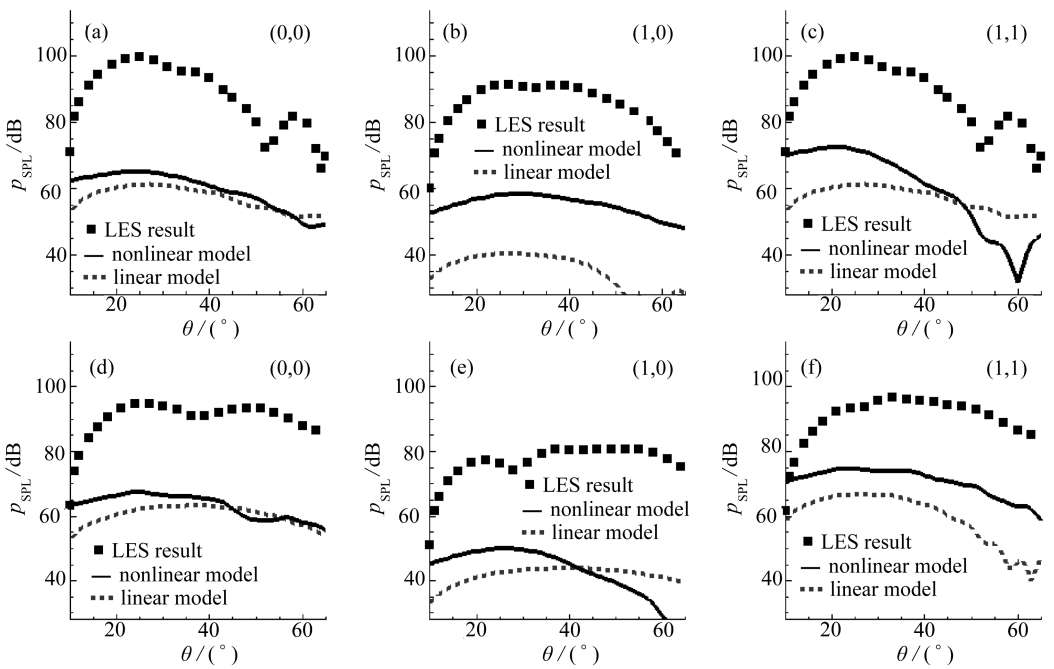

Fig. 7 Sound pressure level vs. polar angle θ at $R = 60r_0$ for different mode combinations ((a)~(c), M08T086[1]; (d)~(f), M08T176)

The far-field acoustic pressure arising from the difference mode interactions corresponding to the maximum amplitude is calculated by Lilley-Goldstein's acoustic analogy. The beam patterns of the heated jet for modes (0, 0), (0, 1) and (1, 1) compared to the corresponding LES patterns are shown in fig. 6. Compared with the beam pattern given by the linear model in fig. 4, the source locations in the near field in the major radiation direction for mode $m = 0$ predicted by the nonlinear model are in better agreement with the LES results. However, it is also worth mentioning that the beam pattern given by the nonlinear model for mode pair (0, 1) is less satisfactory.

In addition, the SPL vs. polar angles given by the present nonlinear model are quantitatively compared with the LES results and the linear model displayed in fig. 7. The far-field sound pressure levels are raised in the nonlinear model at small polar angles compared with those in the linear model in the cold jet[1]. And the enhancement of acoustic efficiency is also found in the present heated jet. More importantly, it is found that the gap of SPL between the LES and the nonlinear model is even reduced. As shown in fig. 7, the SPL for mode pair (1,1) increase even more than those for mode pair (0, 0) in both jets, indicating that mode pair (1,1) has higher acoustic efficiency than (0,0). In short, in the hot jet, the nonlinear interaction of 2 instability waves can increase the acoustic efficiency. For mode $m = 0$, the SPL in the heated jet are slightly increased compared to those in the cold jet. For mode (0, 0) and (1, 1), this enhancement is about 2~3 dB, consistent with the LES results in fig. 2. So this nonlinear model can reflect some features about the effects of heating on sound generation. Large gaps between the nonlinear model and the LES results found in ref. [1] still exist in the present heated jet, but it is reduced to a certain extent. For mode pair (1,0), both the beam pattern and the SPL suggest that this nonlinear model fails to predict the sound for higher difference azimuthal wavenumber Δm.

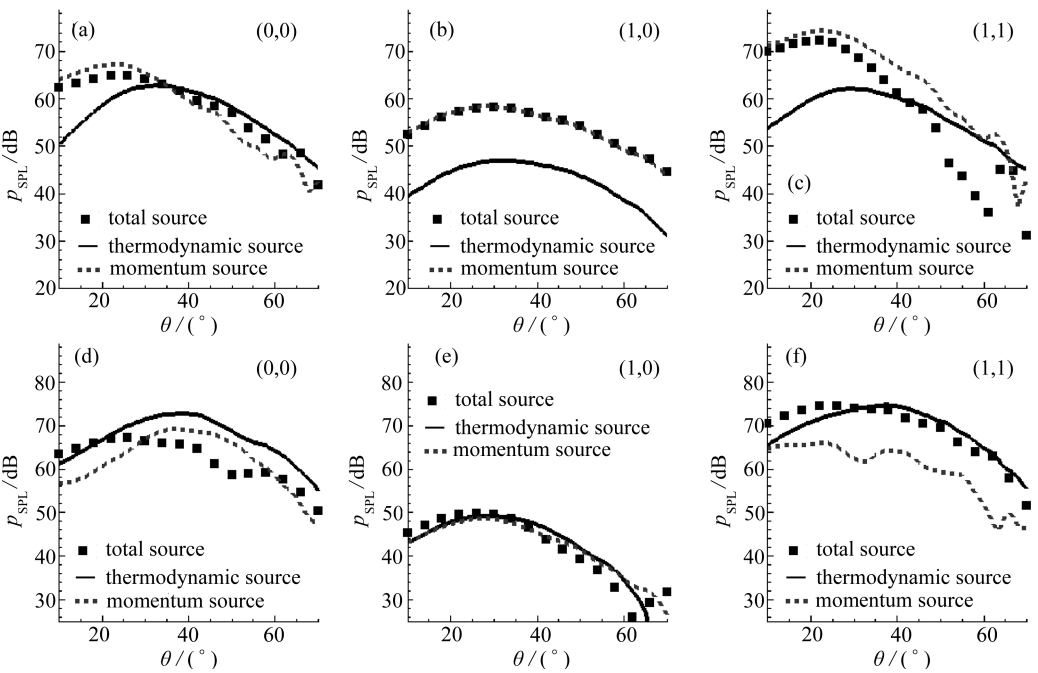

Fig. 8 The sound pressure levels contributed by different sound sources vs. polar angle θ at $R = 60r_0$ ((a)~(c), M08T086; (d)~(f), M08T176)

As aforementioned, some contradictory results from the LES exist in the present nonlinear model. For instance, the lower peak frequency found in the LES sound spectra at polar angle $\theta = 30°$ in the heated jet mismatches the frequency predicted by the nonlinear model. The neglected nonlinear terms in the LPSE, multiple difference frequency combinations

and some other sound generation mechanisms(e.g. sounds from incoherent structures[34]), might cause the mismatching. In a word, the nonlinear model could reproduce some nonlinearities and effects of heating on sound generation by means of instability waves to a certain extent in the heated jet, but it is still unable to predict the far-field SPL accurately due to missing factors in the model.

To further clarify the effects of heating in present subsonic transitional jets, the source terms in the right-hand side of eq.(5) in Lilley-Goldstein's equations are decomposed into two parts, one is the momentum source and the other is the thermodynamic source. The detailed expression of these two sub-sources can be found in ref. [1]. Here, we mainly analyze the contributions to the far-field sound by these two sub-sources respectively and evaluate the effect of heating on sound sources. The SPL contributed by different source components at $R = 60r_0$ of both cold and heated jets are plotted in fig. 8. The sound radiated from the thermodynamic source has higher radiation angles than that from the total source, reaching nearly $\theta = 40°$ for mode pair (0, 0). It is obvious that in the cold jet, the momentum source component plays a dominant role while the thermodynamic component has little contribution to the total source. Especially, for higher azimuthal mode pair (1,0), the total source and the momentum source give almost the same contribution, and the SPL contributed by the thermodynamic source is nearly 13 dB lower than that by the total source. However, in the heated jet, on the contrary, the thermodynamic source term is the most significant part according to fig. 8(d) and (f). For mode pair (1, 0), the contributions from these two sub-source terms are nearly the same. Furthermore, it seems that the contribution by the thermodynamic source is weakened with the increase of m. In other words, the effects of heating are mainly reflected in axisymmetric mode $m = 0$.

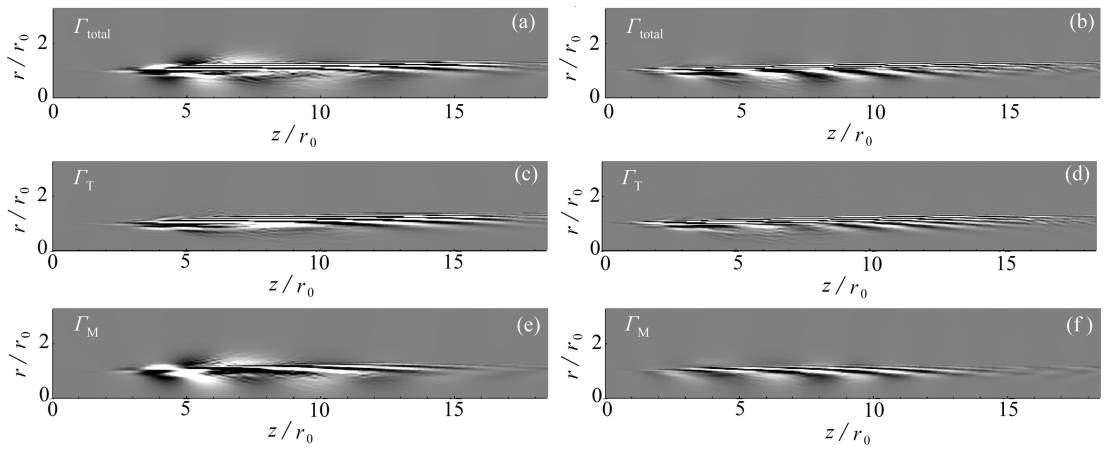

Fig. 9 Contours of real parts of sound sources in the near-field region for mode (0,0) ((a),(c),(e), M08T086; (b),(d),(f), M08T176. The contour levels are [−0.000 1, 0.000 1] in M08T086 and [−0.000 5, 0.000 5] in M08T176)

The different sound sources for mode (0, 0) are displayed in fig. 9. It is found that the

sources are mainly located at $r = r_0$ and $z < 20r_0$. The sound sources decay rapidly along the radial direction, this trend is further enhanced by heating and the peak regions of source terms move closer to the jet outlet. In the cold jet, the momentum source in the potential core dominates the total source, as shown in fig. 9(a) and (e), while the thermodynamic source contributes more in the downstream region. However in the heated jet, not only the whole amplitudes increases, but also the thermodynamic source exceeds the momentum source, especially at $z < 6r_0$, $r = r_0$, that dominates in the total source. In general, the increase of sound pressure levels in the nonlinear model results mainly from the increased contribution by the thermodynamic source.

3 Conclusion

Sound generation in a heated subsonic transitional jet is investigated with the linear parabolized stability equations and Lilley-Goldstein's equations based on the LES database. The linear and nonlinear models addressed in ref. [1] are applied to the present heated jet, and quantitative comparison with the LES results is also carried out to examine to what extent these simplified models could predict the far-field sound in the heated jet, and the effect of heating is particularly investigated.

In the linear model, the maximum-radiation polar angle of the heated jet is higher than that of the cold jet at same frequencies, and the SPL at high frequencies are relatively higher, consistent with the LES and LST results. Compared with that in the cold jet, the gap of SPL between the linear model and the LES is reduced in the heated jet. Similarly, the nonlinear model could predict more accurate maximum radiation angles than the linear model and raise the strength of sound radiation in all cases. For mode $m = 0$, the SPL of the heated jet are 2~3 dB higher than those of the cold jet, and the gap between the nonlinear model and the LES results is also smaller, which accurately reflects the effects of heating on the SPL. In addition, from the perspective of sound sources, the increase of the contribution by the thermodynamic source terms is the main cause for the enhancement of SPL in the heated jet, especially for mode $m = 0$. The thermodynamic source plays a more important role than the momentum source in the heated jet, in contrary in the cold jet.

As a matter of fact, the present transitional jets are different from experimental conditions, and the sound generation mechanisms in fully turbulent jets are even more complicated, so that the incoherent structures neglected in this work might also have great effects on the sound radiation. This is a subject for research in progress.

Acknowledgement

This work was supported by the National Natural Science Foundation of China (11232011; 11402262; 11621202) and the Fundamental Research Funds for the Central Universities.

References:

[1] WAN Zhen-hua, YANG Hai-hua, ZHANG Xing-chen, SUN De-jun. Instability waves and aerodynamic noise in a subsonic transitional turbulent jet[J]. *European Journal of Mechanics—B/Fluids*, 2016, **57**: 192-203.

[2] Tam C K W, Viswanathan K, Ahuja K K, Panda J. The sources of jet noise: experimental evidence[J]. *Journal of Fluid Mechanics*, 2008, **615**: 253-292.

[3] Bishop K A, Ffowcs W J E, Smith W. On the noise sources of the unsuppressed high-speed jet[J]. *Journal of Fluid Mechanics*, 1971, **50**(1): 21-31.

[4] Tam C K W. Directional acoustic radiation from a supersonic jet generated by shear layer instability[J]. *Journal of Fluid Mechanics*, 1971, **46**(4): 757-768.

[5] Suzuki T, Colonius T. Instability waves in a subsonic round jet detected using a near-field phased microphone array[J]. *Journal of Fluid Mechanics*, 2006, **565**: 197-226.

[6] Jordan P, Colonius T. Wave packets and turbulent jet noise[J]. *Annual Review of Fluid Mechanics*, 2013, **45**: 173-195.

[7] Cavalieri A V G, Jordan P, Agarwal A, Gervais Y. Jittering wave-packet models for subsonic jet noise[J]. *Journal of Sound and Vibration*, 2011, **330**(18/19): 4474-4492.

[8] Cavalieri A V G, Daviller G, Comte P, Jordan P, Tadmor G, Gervais Y. Using large eddy simulation to explore sound-source mechanisms in jets[J]. *Journal of Sound and Vibration*, 2011, **330**(17): 4098-4113.

[9] Cavalieri A V G, Rodríguez D, Jordan P, Colonius T. Wavepackets in the velocity field of turbulent jets[J]. *Journal of Fluid Mechanics*, 2013, **730**: 559-592.

[10] Cavalieri A V G, Agarwal A. Coherence decay and its impact on sound radiation by wavepackets[J]. *Journal of Fluid Mechanics*, 2014, **748**: 399-415.

[11] Rodríguez D, Cavalieri A V G, Colonius T, Jordan P. A study of linear wavepacket models for subsonic turbulent jets using local eigenmode decomposition of PIV data[J]. *European Journal of Mechanics—B/Fluids*, 2015, **49**(B): 308-321.

[12] Cheung L C. Aeroacoustic noise prediction and the dynamics of shear layers and jets using the nonlinear parabolized stability equations[D]. Stanford University, 2007.

[13] Bertolotti F P, Herbert Th. Analysis of the linear stability of compressible boundary layers using the PSE[J]. *Theoretical and Computational Fluid Dynamics*, 1991, **3**(2):117-124.

[14] Bertolotti F P, Herbert Th, Spalart P R. Linear and nonlinear stability of the Blasius boundary layer[J]. *Journal of Fluid Mechanics*, 1992, **242**: 441-474.

[15] Rodríguez D, Sinha A, Brès G A, Colonius T. Parabolized stability equation models in turbulent supersonic jets[C]//*18th AIAA/CEAS Aeroacoustics Conference* (*33rd AIAA Aeroacoustics Conference*). 2012: AIAA-2012-2117.

[16] Sinha A, Rodríguez D, Brès G A, Colonius T. Wavepacket models for supersonic jet noise [J]. *Journal of Fluid Mechanics*, 2014, **742**: 71-95.

[17] Sandham N D, Morfey C L, Hu Z W. Nonlinear mechanisms of sound generation in a perturbed parallel jet flow[J]. *Journal of Fluid Mechanics*, 2006, **565**:1-23.

[18] Sandham N D, Salgado A M. Nonlinear interaction model of subsonic jet noise[J]. *Philosophical Transactions*, *Series A*, *Mathematical*, *Physical*, *and Engineering Sciences*, 2008, **366** (1876): 2745-2760.

[19] WAN Zhen-hua, ZHOU Lin, YANG Hai-hua, SUN De-jun. Large eddy simulation of flow devel-

opment and noise generation of free and swirling jets[J]. *Physics of Fluids*, 2013, **25**(12): 126103.

[20] Herbert Th. Parabolized stability equations[J]. *Annual Review of Fluid Mechanics*, 1997, **29**: 245-283.

[21] Andersson P, Henningson D S, Hanifi A. On a stabilization procedure for the parabolic stability equations[J]. *Journal of Engineering Mathematics*, 1998, **33**(3): 311-332.

[22] Lilley G M. On the noise from jets[C]//*Noise Mechanisms*. 1974: Agard cp-131.

[23] Goldstein M E. An exact form of Lilley's equation with a velocity quadrupole/temperature dipole source term[J]. *Journal of Fluid Mechanics*, 2001, **443**: 231-236.

[24] Ray P K, Lele S K. Sound generated by instability wave/shock-cell interaction in supersonic jets[J]. *Journal of Fluid Mechanics*, 2007, **587**: 173-215.

[25] Bodony D J, Lele S K. On using large-eddy simulation for the prediction of noise from cold and heated turbulent jets[J]. *Physics of Fluids*, 2005, **17**(8): 085103.

[26] Mollo-Christensen E, Kolpin M A, Martuccelli J R. Experiments on jet flows and jet noise far-field spectra and directivity patterns[J]. *Journal of Fluid Mechanics*, 1964, **18**(2): 285-301.

[27] Lush P A. Measurements of subsonic jet noise and comparison with theory[J]. *Journal of Fluid Mechanics*, 1971, **46**(3): 477-500.

[28] Stromberg J L, McLaughlin D K, Troutt T R. Flow field and acoustic properties of a Mach number 0.9 jet at a low Reynolds number[J]. *Journal of Sound and Vibration*, 1980, **72**(2): 159-176.

[29] Tanna H K. An experimental study of jet noise part I: turbulent mixing noise[J]. *Journal of Sound and Vibration*, 1977, **50**(3): 405-428.

[30] Bogey C, Barré S, Fleury V, Bailly C, Juvé D. Experimental study of the spectral properties of near-field and far-field jet noise[J]. *Int J Aeroacoust*, 2007, **6**(2): 73-92.

[31] Suponitsky V, Sandham N D, Agarwal A. On the Mach number and temperature dependence of jet noise: results from a simplified numerical model[J]. *Journal of Sound and Vibration*, 2011, **330**(17): 4123-4138.

[32] Cavalieri A V G, Jordan P, Colonius T, Gervais Y. Axisymmetric superdirectivity in subsonic jets[J]. *Journal of Fluid Mechanics*, 2012, **704**: 388-420.

[33] Suponitsky V, Sandham N D, Morfey C L. Linear and nonlinear mechanisms of sound radiation by instability waves in subsonic jets[J]. *Journal of Fluid Mechanics*, 2010, **658**: 509-538.

[34] Towne A, Colonius T, Jordan P, Cavalieri A V, Brès G A. Stochastic and nonlinear forcing of wavepackets in a Mach 0.9 jet[C]//*21st AIAA/CEAS Aeroacoustics Conference*. Dallas, TX, 2015: AIAA-2015-2217.

亚声速热射流声源模型的应用

张星辰， 杨海华， 万振华， 孙德军

（中国科学技术大学 近代力学系，合肥 230027）

摘要： 对亚声速转捩热射流中失稳波相关的噪声产生机制进行了研究，并与冷射流中的结果进行了对比.基于时均大涡模拟（LES）流场，通过求解线性抛物化稳定性方程（LPSE）得到了失稳波的空间演化特性，然后基于 LPSE 的解与声比拟方法构建了射流的线性及非线性声源模型.LPSE 结果表明，加热可以提高失稳波的空间增长率，使其更早达到饱和.由线性模型分析可知，加热会提高高频模态的声压级（SPL）.与冷射流相比，热射流中线性模型预测的声压级与大涡模拟结果间的差距更小，表明线性机制在热射流中作用更大.在亚声速冷射流中，非线性模型在之前的研究中已经被证明可以提高声辐射效率.在当前热射流中，发现非线性模型与大涡模拟间的声压级差距被进一步的缩小，且温度相关的声源项在声辐射中发挥更重要的作用.

关 键 词： 线性抛物化稳定性方程； 失稳波； 线性机制； 非线性机制

基金项目： 国家自然科学基金（11232011；11402262；11621202）

引用本文/Cite this paper：

ZHANG Xing-chen, YANG Hai-hua, WAN Zhen-hua, SUN De-jun. Application of sound source models to the heated subsonic jet[J]. *Applied Mathematics and Mechanics*, 2016, **37**(12): 1308-1323.

张星辰，杨海华，万振华，孙德军. 亚声速热射流声源模型的应用[J]. 应用数学和力学，2016，**37**(12)：1308-1323.